Secondary oxidation product on Si(111)-(7×7) characterized by isotope-labeled vibrational spectroscopy

H. Okuyama,[a] Y. Ohtsuka, and T. Aruga
Department of Chemistry, Graduate School of Science, Kyoto University, Kyoto 606-8502, Japan

(Received 17 February 2005; accepted 25 April 2005; published online 22 June 2005)

The reaction of O_2 with Si(111)-(7×7) has been studied by electron energy-loss spectroscopy at 82 K. In addition to the losses due to Si–O–Si configurations, we observed two Si–O stretch modes depending on the coverage. A 146-meV peak appears at the initial reaction stage and was ascribed to a metastable product with one oxygen atom bonding on top of Si adatom and the other inserted into the backbond. The initial product is further oxidized to produce the second Si–O stretch peak at 150 meV. The secondary product was partially substituted with isotopes and analyzed with a simple model of coupled oscillators. The vibrational spectra reflect dynamical couplings between the isotopes, which is consistent with those predicted from the tetrahedral SiO_4 structure with one on top and three inserted oxygen atoms. © *2005 American Institute of Physics*.
[DOI: 10.1063/1.1937394]

I. INTRODUCTION

As a consequence of device miniaturization, silicon oxide will be scaled down to thickness of only a few atomic layers.[1] Initial oxidation of silicon surfaces has been studied for the atomic-scale understanding of the oxide formation process. Over the last three decades, the reaction of O_2 gas with Si(111)-(7×7) has been studied by many researchers from both experimental[2–22] and theoretical[23–28] points of view. A controversy arised from an equivocal assignment of the metastable 150-meV vibrational peak observed by electron energy-loss spectroscopy (EELS). The 150-meV peak was initially assigned to the internal mode of molecular species,[2,3] which was supported by photoemission[4] and work-function measurement.[6]

On the other hand, Schell-Sorokin and Demuth[5] proposed assigning the peak to the diatomiclike silicon monoxide (SiO species). By employing density-functional theory, Lee and Kang[25] suggested that the 150-meV vibrational peak is indeed attributable to the Si–O stretch mode. They proposed that the ad-ins structure [Fig. 1(a)] is thermally metastable and is a candidate for an initial product at low temperature. The notations "ad" and "ins" represent an oxygen atom bonded on top of Si adatom and that inserted into a backbond, respectively. The absence of molecular state was supported by reactive Cs^+ ion scattering experiment, which detected no $CsSiO_2^+$ or CsO_2^+ as a scattering product.[11] Comtet *et al.* observed O^+ ion as a photodesorption product,[15] which was attributed to the on-top SiO species based on the comparative analysis with electron photoemission spectra. The recent EELS study provided spectroscopic evidence that the initial reaction results in the ad-ins structure at 82 K.[20]

It was proposed that the metastable ad-ins structure transforms into ins×2 structure [Fig. 1(b)] by thermal activation.[15,19,20,25] The ad-ins and ins×2 products were imaged by scanning tunneling microscope (STM) at 78 K (Refs. 17, 20, and 22) and 30 K,[19] which appears dark and bright at the adatom sites, respectively, in agreement with the theoretical predictions.[24,25] Thus, by recent studies of both theories and experiments, it is now a consensus that the initial oxidation product on Si(111)-(7×7) is the ad-ins-type at ~80 K which converts to the stable ins×2 structure at higher temperature [200 K (Ref. 20)].

The initial products are further oxidized with increasing the exposure, although the structure remains controversial. Several photoemission studies proposed that the molecular configuration is possible as a secondary product at ~100 K (Refs. 12, 16, and 18) and 300 K,[14,18,21] and that the structure is stabilized against the dissociation by the inserted oxygen atom. Although the temperature reported was different, the x-ray-absorption study showed distinct molecular feature only below 200 K.[13] The molecular configuration, however, was not consistent with the theories, which proposed that it spontaneously dissociates, yielding a tetrahedral SiO_4 structure denoted by ad-ins×3 [Fig. 1(c)].[23,26] Comtet *et al.*[15] supported the SiO_4 structure by analyses of O^+ photodesorption yield as a function of temperature, coverage, and photon energy. The photodesorption yield showed resonances at the same energies as those observed for silicon oxide, which suggested the tetrahedral atomic arrangement of oxygen atoms. The discrepancy was suggested to arise from the ambiguity in the assignment of the photoemission peak to the specific configuration of the product.[29] In this study, we studied the secondary product by means of isotope-labeled vibrational spectroscopy at 82 K. The secondary product was partially substituted with the isotope and the vibrational spectra were analyzed with the model of coupled oscillators, which enabled us to convincingly assign the secondary product as the ad-ins×3 structure.

[a]Electronic mail: hokuyama@kuchem.kyoto-u.ac.jp

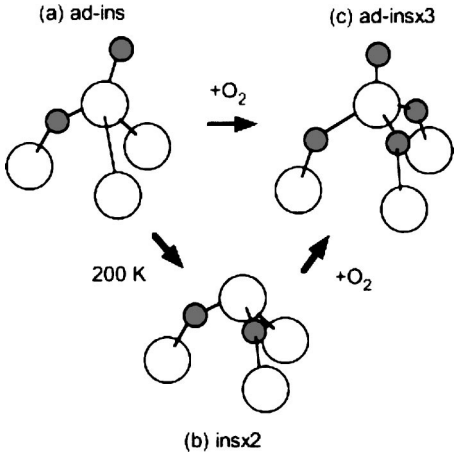

FIG. 1. Schematic model of oxidation reaction on Si(111)-(7×7). The open and gray circles indicate the Si and O atoms, respectively. The initial product at 82 K is of the ad-ins type which transforms to the ins×2 structure at 200 K. It was proposed that the successive reaction with further O_2 produces the ad-ins×3 structure (Refs. 23 and 26).

II. EXPERIMENTS

The experiments were carried out in an ultrahigh-vacuum (UHV) chamber equipped with a high-resolution electron energy-loss spectrometer (LK-5000, LK Technologies, Inc.) and a four-grid retarding-field analyzer for low-energy electron diffraction (LEED). The base pressure of the chamber was below 1×10^{-10} Torr. For the EELS measurements, the incidence angle $\theta_i=60°$, reflection angle $\theta_r=60°$, and energy resolution of 3–4 meV (the full width at half maximum of the elastic peak) were used. The scattering plane was aligned along the $[01\bar{1}]$ direction. The angle-dependent measurements revealed that the dipole scattering is responsible for the observed losses.[30]

The silicon used in the experiments was cut from an *n*-type, As-doped wafer, which was cleaned by the overnight degassing at 900 K, followed by the flashing up to 1500 K. For a clean surface, a sharp (7×7) LEED pattern was observed and EELS showed no trace of impurity. We used isotope gasses of $^{16}O_2$ and $^{18}O_2$ with the purities of 99.9% and 99%, respectively. The sample was exposed to $^{16}O_2$ and/or $^{18}O_2$ via two different tube dosers which were positioned ~1 cm apart from the sample surface. Exposures are given by background O_2 pressure multiplied by time in units of langmuir (1 L=1×10^{-6} Torr s). The actual exposure was larger than indicated due to the use of dosers by a factor of ~7. The exposure and EELS measurements were conducted at 82 K.

III. RESULTS AND DISCUSSION

A series of EELS spectra of $^{16}O_2$/Si(111)-(7×7) are shown in Fig. 2 as a function of the exposure. At the initial-stage reaction, two peaks appear at 80 and 146 meV [(b) and (c)]. As the exposure increases to 0.03 L, two peaks start to develop at 128 and 150 meV (d). It was already established that the 80- and 128-meV losses are ascribed to the Si–O–Si symmetric and asymmetric stretch modes, respectively.[2] The 146- and 150-meV peaks, denoted by ν_1 and ν_2, respectively, were assigned to the Si–O stretch modes.[20] The initial features at 80 and 146 meV were assigned to the Si–O–Si and Si–O stretch modes, respectively, of the ad-ins structure.[20] The exposure dependences of the ν_1 and ν_2 peaks are shown in the inset. The ν_1 peak grows at first and then attenuates in intensity, accompanied with the growth of the ν_2 peak. This result suggests that the initial product is further oxidized to yield the secondary product. The secondary product is characterized by ν_2 and two Si–O–Si stretch modes at 80 and 128 meV. At 0.1–0.2 L, the 128-meV peak is broadened and shifts to 129 meV. Also a broad structure is observed around 70–100 meV, indicating that the surface is inhomogeneous with various Si–O–Si configurations.

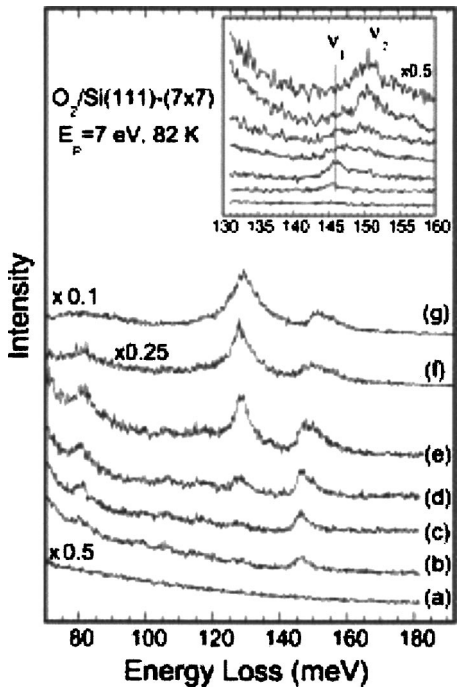

FIG. 2. EELS spectra of Si(111)-(7×7) as a function of the exposure to $^{16}O_2$ taken at $E_p=7$ eV. The exposures are (a) 0, (b) 0.01, (c) 0.02, (d) 0.03, (e) 0.07, (f) 0.1, and (g) 0.2 L. The inset shows the inspect of the Si–O stretch region taken with another sample at $E_p=8$ eV. The exposures are 0.01, 0.02, 0.04, 0.06, 0.08, 0.1, and 0.15 L from the bottom to the top. The loss intensities are normalized to the elastic peak intensities.

The temperature effect of the initial product is shown in Fig. 3. The clean surface was exposed to 0.02-L $^{16}O_2$ at 82 K, and two peaks appear at 80 and 146 meV due to the initial product [spectrum (a)]. The sample was subsequently annealed to 200 K and then cooled to 82 K [spectrum (b)]. The ν_1 peak disappears and two losses are observed at 81 and 104 meV. Spectrum (b′) was taken after a similar sample preparation except for the use of the $^{18}O_2$ isotope, which exhibits losses at 80 and 100 meV. Although the signal-to-noise ratio is not sufficiently high, the isotope shifts ensure that these two peaks are derived from oxygen. The disappearance of the ν_1 peak suggests that the metastable on-top oxygen migrates into the backbond to form the ins×2 structure by thermal activation.[25] For the ins×2 structure, it is anticipated that the two inserted oxygen atoms are dynamically coupled and the Si–O–Si symmetric and asymmetric stretch modes are further classified by in-phase and out-of-phase motions. The theory predicted the vibrational energies of the in-phase symmetric and asymmetric stretch

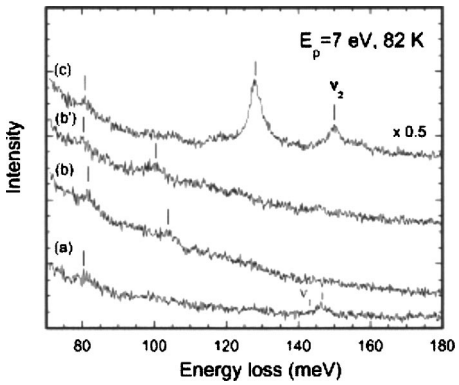

FIG. 3. (a) An EELS spectrum of Si(111)-(7×7) exposed to 0.02-L $^{16}O_2$ at 82 K. The 80- and 146-meV losses are characteristic of the ad-ins product. (b) The surface was subsequently heated to 200 K. The ν_1 peak disappears and two peaks are observed at 81 and 104 meV, which are ascribed to the ins×2 product. (b′) The corresponding spectrum taken with $^{18}O_2$, which exhibits isotope-shifted peaks at 80 and 100 meV. (c) The surface after annealing [spectrum (b)] was further exposed to 0.02-L $^{16}O_2$. The 80-, 128-, and 150-meV peaks are characteristic of the secondary product.

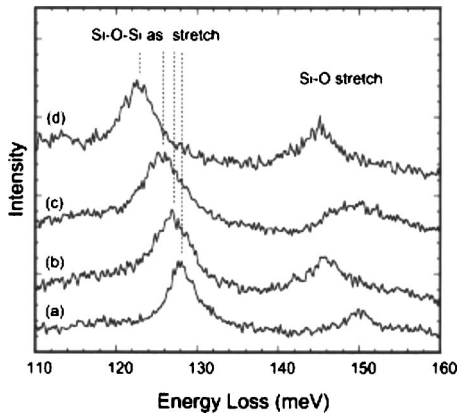

FIG. 4. Isotope-labeled EELS spectra of the secondary oxidation products prepared by way of the two-step reaction: The clean surface was exposed to 0.02-L $^{16}O_2$ [(a) and (b)] or $^{18}O_2$ [(c) and (d)], and subsequently heated to 200 K. Then the surface was further exposed to 0.02-L $^{16}O_2$ [(a) and (c)] or $^{18}O_2$ [(b) and (d)]. The Si–O stretch mode is associated with the postexposed isotope. The Si–O–Si asymmetric stretch modes show energy shifts depending on the isotopic combinations due to dynamical couplings.

modes to be 78 and 97 meV, respectively.[26] We assign the 81(80)- and 104(100)-meV peaks to the in-phase symmetric and asymmetric stretch modes, respectively. The out-of-phase modes are forbidden according to the surface selection rule of dipole scattering.[30] The experimental energies for the initial and secondary products are summarized in Table I.

The secondary product results from subsequent oxidation of the ad-ins product as shown in Fig. 2. The ν_1 peak disappears and the ν_2 peak becomes dominant at 0.1 L, where the Si–O–Si stretch peaks are significantly broadened due to the surface inhomogeneity. We found that the secondary species can be readily produced via the ins×2 structure. The surface after annealing [spectrum (b) in Fig. 3] was further exposed to 0.02-L $^{16}O_2$ at 82 K (total exposure is 0.04 L) [spectrum (c)]. The ν_2 peak appears predominantly in the Si–O stretch region without significant contribution of the ν_1 peak. Furthermore, the Si–O–Si asymmetric stretch peak at 128 meV is relatively sharp, indicating higher homogeneity of the product. Although there may exist unreacted ins×2 species, it gives no vibrational feature at 120–150 meV. These results suggest that the postexposed oxygen reacts preferentially with the ins×2 species: The ins×2 species is more reactive to incoming O_2 than the ad-ins species and possibly even unreacted Si adatoms. The high reactivity of the ins×2 species is corroborated by the STM observation that a bright site (ins×2) is reactive toward the incoming O_2 to produce a dark site (secondary product).[7,9]

TABLE I. A summary of experimental energies (meV) with $^{16}O_2$ ($^{18}O_2$) and mode assignments for the structures shown in Fig. 1.

Structure	Energy (meV)	Assignment
ad-ins	80(78)	Si–O–Si stretch (s)
⋯	146(142)	Si–O stretch, ν_1
ins×2	81(80)	Si–O–Si stretch (s)
⋯	104(100)	Si–O–Si stretch (as)
ad-ins×3	80(78)	Si–O–Si stretch (s)
⋯	128–129(122–123)	Si–O–Si stretch (as)
⋯	150(145)	Si–O stretch, ν_2

The secondary product is characterized by one Si–O stretch mode (ν_2) and two Si–O–Si stretch modes at 80 and 128 meV. The exposure dependence of the ν_1 and ν_2 peaks (Fig. 2) suggests that the secondary product is the ad-ins ×3 type. Then the 80- and 128-meV peaks are assigned to the Si–O–Si symmetric and asymmetric stretch modes of the three inserted oxygen. To make a clearer assignment, the secondary product was partially substituted with oxygen isotope by way of the two-step reaction demonstrated in Fig. 3. For example, the clean Si(111)-(7×7) surface was exposed to 0.02-L $^{16}O_2$ and subsequently heated to 200 K, which yields only ins^{16}×2 species on the surface. The surface was subsequently exposed to 0.02-L $^{18}O_2$ at 82 K to produce the secondary species. In this way, we prepared the surface with four different procedures as $^{16}O_2 \rightarrow 200\ K \rightarrow {}^{16}O_2$, $^{16}O_2 \rightarrow 200\ K \rightarrow {}^{18}O_2$, $^{18}O_2 \rightarrow 200\ K \rightarrow {}^{16}O_2$, and $^{18}O_2 \rightarrow 200\ K \rightarrow {}^{18}O_2$. The corresponding EELS spectra are shown in Fig. 4. For the secondary product constituted with only ^{16}O, the Si–O–Si asymmetric and Si–O stretch modes are observed at 128.1±0.2 and 150 meV, respectively [spectrum (a)]. When completely substituted with ^{18}O, the secondary product shows corresponding downshifted peaks at 122.8±0.2 and 145 meV. In the case of partial substitutions, the Si–O stretch modes are observed at 146 and 150 meV for (b) and (c), respectively, indicating that the postexposed oxygen dissociates and one bonds on top of Si adatom. Furthermore, the Si–O–Si asymmetric stretch modes appear at 127.1±0.2 and 125.7±0.2 meV for (b) and (c), respectively, which lie in the intermediate of (a) and (d). The result indicates that this mode is associated with both pre- and postexposed isotopes; the dissociated counterpart of the postexposed isotope is inserted into the intact backbond. The multiply inserted oxygen atoms causes dynamical coupling of the Si–O–Si stretch vibration, giving rise to different normal modes depending on the isotopic combinations. Thus the spectra are quite consistent with the assignment that the secondary product is of the ad-ins×3 type.

To make a quantitative analysis of the vibrational spectra, three coupled oscillators are considered as a model of the Si–O–Si asymmetric stretch vibrations of the ad-ins$\times$3 structure. Within the harmonic approximation, the Hamiltonian is represented by

$$H = \sum_{i=1}^{3} \epsilon_i c_i^{\dagger} c_i + \sum_{i,j=1}^{3} \Delta_{i,j} c_i^{\dagger} c_j. \tag{1}$$

The notations of the Hubbard model are used for simple description of the matrix elements, where $c_i^{\dagger}$ (c_i) is the creation (annihilation) operator for the site (oscillator) i. ϵ_i is the vibrational energy of oscillator i without dynamical couplings, and $\Delta_{i,j}$ corresponds to the dynamical interaction between them. We consider ϵ_{16} and ϵ_{18} for Si$-{}^{16}$O$-$Si and Si$-{}^{18}$O$-$Si oscillators, respectively, and interaction parameters $\Delta_{16,16}$, $\Delta_{16,18}$, and $\Delta_{18,18}$ between them.

We treat the interactions perturbatively and start with the local oscillator basis as verified from $\epsilon \gg \Delta$. In the case of ad^{18}-ins$^{16}\times$2-ins^{18} structure, for example, the Hamiltonian is represented by

$$H = \begin{pmatrix} \epsilon_{16} & \Delta_{16,16} & \Delta_{16,18} \\ \Delta_{16,16} & \epsilon_{16} & \Delta_{16,18} \\ \Delta_{16,18} & \Delta_{16,18} & \epsilon_{18} \end{pmatrix}. \tag{2}$$

The matrix can be diagonalized analytically to yield the eigenvalues,

$$E_{1,2} = \frac{\epsilon_{16} + \epsilon_{18} + \Delta_{16,16} \pm \sqrt{\epsilon_{16}^2 + \epsilon_{18}^2 - 2\epsilon_{16}\epsilon_{18} + 2\epsilon_{16}\Delta_{16,16} - 2\epsilon_{18}\Delta_{16,16} + \Delta_{16,16}^2 + 8\Delta_{16,16}^2}}{2},$$

$$E_3 = \epsilon_{16} - \Delta_{16,16}. \tag{3}$$

In a similar way, the eigenvalues were deduced for the other combinations. Among the two or three normal modes for each combination, we consider only totally symmetric modes according to the surface selection rule of dipole scattering. In the above case, two totally symmetric modes appear which are classified as in-phase (E_1) and out-of-phase (E_2) motions. As described below, the EELS intensities for the out-of-phase modes are weak compared to those of the in-phase modes. Thus we fitted the experimental energies to those for the in-phase modes by the method of least square, and determined the parameters to be 124.1 ± 0.2, 119.1 ± 0.2, and 2.0 ± 0.1 meV for ϵ_{16}, ϵ_{18}, and Δ, respectively. Here, we put $\Delta_{16,16}=\Delta$, and approximately $\Delta_{16,18}=\sqrt{\frac{17}{18}}\Delta$ and $\Delta_{18,18}=\sqrt{\frac{16}{18}}\Delta$. The results are presented in Table II and Fig. 5 as a function of Δ. The solid and dashed curves indicate the in-phase and out-of-phase modes, respectively. The experimental energies are plotted by the dots, which are well reproduced by the model.

In the cases of partial substitutions, the out-of-phase modes are predicted to appear at 118.2 and 119.5 meV (dashed curves) for the ins$^{16}\times$2-ins^{18} and ins^{16}-ins$^{18}\times$2 combinations, respectively. The EELS intensity is proportional to the square of the dynamic dipole moment induced by the excitations. The relative dipole moments can be derived from the calculated eigenvectors, which are schematically shown in Fig. 6. The normal components of the total dipole moments are larger for the in-phase mode than the out-of-phase mode by a factor of 3.3 and 2.2 for the ins^{18}-ins$^{16}\times$2 and ins^{16}-ins$^{18}\times$2 configurations, respectively. Thus the corresponding intensity ratios are $\sim$11 and $\sim$5 for the former and latter, respectively, indicating that the out-of-phase counterparts are almost invisible in the spectra.

TABLE II. Energies of the Si–O–Si asymmetric stretch modes observed in the isotope-labeled experiments and the results of the least-squares fitting (meV). The procedure $^{16}O_2+{}^{18}O_2$ indicates that the clean surface was exposed to $^{16}O_2$, heated to 200 K, and subsequently exposed to $^{18}O_2$.

Procedure	Expt.	Fit
$^{16}O_2+{}^{16}O_2$	128.1 ± 0.2	128.1
$^{16}O_2+{}^{18}O_2$	127.1 ± 0.2	127.0
$^{18}O_2+{}^{16}O_2$	125.7 ± 0.2	125.7
$^{18}O_2+{}^{18}O_2$	122.8 ± 0.2	122.9

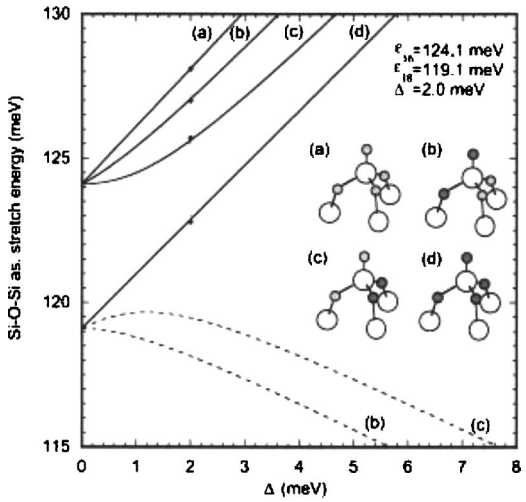

FIG. 5. The calculated energies of the Si–O–Si asymmetric stretch modes as a function of the interaction parameter Δ. The isotopic combinations are (a) ins$^{16}\times$3, (b) ins^{18}-ins$^{16}\times$2, (c) ins^{16}-ins$^{18}\times$2, and (d) ins$^{18}\times$3. The schematic structures are depicted in the inset, where the open, gray, and black circles indicate Si, ^{16}O, and ^{18}O atoms, respectively. The solid and dashed curves correspond to the in-phase and out-of-phase modes, respectively. For (a) and (d), the out-of-phase modes are dipole forbidden and thus are not presented. The experimental energies are shown by the dots, and the parameters ϵ_{16}, ϵ_{18}, and Δ were determined by the least-squares fitting.

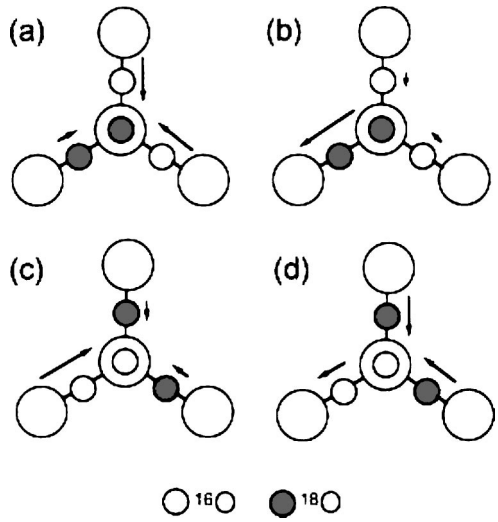

FIG. 6. Schematic of the Si–O–Si asymmetric stretch vibrations of the [(a) and (b)] ad^{18}-ins^{18}-$ins^{16}\times 2$ and [(c) and (d)] ad^{16}-ins^{16}-$ins^{18}\times 2$ structures. The large open circles indicate Si atoms, and the small gray and black circles indicate ^{16}O and ^{18}O atoms, respectively. The normal modes are represented by the [(a) and (c)] in-phase and [(b) and (d)] out-of-phase motions of the oxygen atoms. The arrows are depicted with its length proportional to the dynamic dipole moment induced by the excitations.

It is noted that the Si adatom belongs to the C_s point group (slightly distorted from C_{3V} due to the surface reconstruction). The distortion may cause inhomogeneous broadening of the vibrational peaks in the case of partial substitutions. However, no significant broadenings were observed as compared to the spectra for the pure isotopes, verifying that the distortion is negligible and three inserted oxygen can be treated almost equivalently in the calculation of the normal modes. As a whole, the vibrational energies of the isotope-labeled experiments are well reproduced by the model of three coupled oscillators, which enabled us to unequivocally assign the secondary product as the ad-ins$\times 3$ structure.

IV. SUMMARY

The secondary oxidation product on Si(111)-(7×7) was investigated at 82 K by isotope-labeled EELS. The Si–O–Si asymmetric stretch mode was analyzed with partial isotopic substitution. The vibrational spectra can be explained by considering dynamical couplings between three inserted oxygen atoms, and thus, the secondary product was convincingly assigned as the ad-ins$\times 3$ structure. The result further indicates that the reaction scheme shown in Fig. 1 is established as an initial oxidation process of Si(111)-(7×7).

ACKNOWLEDGMENT

This work was supported in part by a Grant-in-Aid from the Ministry of Education, Science, Sports and Culture (Japan).

[1] J. Dąbrowski and H.-J. Müssig, *Silicon Surfaces and Formation of Interfaces* (World Scientific, Singapore, 1999).
[2] H. Ibach, H. D. Bruchmann, and H. Wagner, Appl. Phys. A: Solids Surf. **29**, 113 (1982).
[3] K. Edamoto, Y. Kubota, H. Kobayashi, M. Onchi, and M. Nishijima, J. Chem. Phys. **83**, 428 (1985).
[4] U. Höfer, P. Morgen, W. Wurth, and E. Umbach, Phys. Rev. Lett. **55**, 2979 (1985).
[5] A. J. Schell-Sorokin and J. E. Demuth, Surf. Sci. **157**, 273 (1985).
[6] C. Silvestre and M. Shayegan, Phys. Rev. B **37**, 10432 (1988).
[7] J. P. Pelz and R. H. Koch, J. Vac. Sci. Technol. B **9**, 424 (1991).
[8] R. Martel, Ph. Avouris, and I.-W. Lyo, Science **272**, 385 (1996).
[9] G. Dujardin, A. Mayne, G. Comtet, L. Hellner, M. Jamet, E. Le Goff, and P. Millet, Phys. Rev. Lett. **76**, 3782 (1996).
[10] I.-S. Hwang, R.-L. Lo, and T. T. Tsong, Phys. Rev. Lett. **78**, 4797 (1997).
[11] K.-Y. Kim, T.-H. Shin, S.-J. Han, and H. Kang, Phys. Rev. Lett. **82**, 1329 (1999).
[12] K. Sakamoto, S. Doi, Y. Ushimi, K. Ohno, H. W. Yeom, T. Ohta, S. Suto, and W. Uchida, Phys. Rev. B **60**, R8465 (1999).
[13] F. Matsui, H. W. Yeom, K. Amemiya, K. Tono, and T. Ohta, Phys. Rev. Lett. **85**, 630 (2000).
[14] T. Jensen, L.-B. Tækker, C. Gundlach, F. K. Dam, P. Morgen, S. V. Hoffman, Z. Li, and K. Pedersen, Phys. Rev. B **64**, 045304 (2001).
[15] G. Comtet, L. Hellner, G. Dujardin, and K. Bobrov, Phys. Rev. B **65**, 035315 (2002).
[16] K. Sakamoto, F. Matsui, M. Hirano, H. W. Yeom, H. M. Zhang, and R. I. G. Uhrberg, Phys. Rev. B **65**, 201309 (2002).
[17] H. Okuyama, T. Miki, T. Aruga, and M. Nishijima, Jpn. J. Appl. Phys., Part 2 **41**, L1419 (2002).
[18] K. Sakamoto, H. M. Zhang, and R. I. G. Uhrberg, Phys. Rev. B **68**, 075302 (2003).
[19] A. J. Mayne, F. Rose, G. Comtet, L. Hellner, and G. Dujardin, Surf. Sci. **528**, 132 (2003).
[20] H. Okuyama, T. Aruga, and M. Nishijima, Phys. Rev. Lett. **91**, 256102 (2003).
[21] K. Sakamoto, H. M. Zhang, and R. I. G. Uhrberg, Phys. Rev. B **70**, 035301 (2004).
[22] Y. Konishi, S. Yoshida, Y. Sainoo, O. Takeuchi, and H. Shigekawa, Phys. Rev. B **70**, 165302 (2004).
[23] B. Schubert, Ph. Avouris, and R. Hoffmann, J. Chem. Phys. **98**, 7593 (1993); J. Chem. Phys. **98**, 7606 (1993).
[24] H. Kageshima, Y. Ono, M. Tabe, and T. Ohno, Jpn. J. Appl. Phys., Part 1 **33**, 4070 (1994).
[25] S.-H. Lee and M.-H. Kang, Phys. Rev. Lett. **82**, 968 (1999).
[26] S.-H. Lee and M.-H. Kang, Phys. Rev. B **61**, 8250 (2000).
[27] T. Hoshino and Y. Nishioka, Phys. Rev. B **61**, 4705 (2000).
[28] M.-H. Tsai, Y.-H. Tang, I.-S. Hwang, and T. T. Tsong, Phys. Rev. B **66**, 241304 (2002).
[29] H. W. Yeom, Phys. Rev. B **66**, 157301 (2002).
[30] H. Ibach and D. L. Mills, *Electron Energy-Loss Specroscopy and Surface Vibrations* (Academic, New York, 1982).